A MS-CASPT2 study of the low-lying electronic excited states of CH 2BrCl

ARTICLE *in* CHEMICAL PHYSICS LETTERS · DECEMBER 2001

Impact Factor: 1.9 · DOI: 10.1016/S0009-2614(01)01273-8

3 AUTHORS, INCLUDING:

Tamás Rozgonyi
Hungarian Academy of Sciences
39 PUBLICATIONS **304** CITATIONS
SEE PROFILE

Leticia González
University of Vienna
210 PUBLICATIONS **3,376** CITATIONS
SEE PROFILE

14 December 2001

Chemical Physics Letters 350 (2001) 155–164

CHEMICAL PHYSICS LETTERS

www.elsevier.com/locate/cplett

A MS-CASPT2 study of the low-lying electronic excited states of CH_2BrCl

Tamás Rozgonyi [a,1], Thomas Feurer [a], Leticia González [b,*]

[a] *Institut für Optik und Quantenelektronik, Max-Wien-Platz 1, D-07743 Jena, Germany*

[b] *Institut für Chemie, Physikalische und Theoretische Chemie, Freie Universität Berlin, Takustrasse 3, D-14195 Berlin, Germany*

Received 30 August 2001; in final form 18 October 2001

Abstract

The low-lying singlet excited states of CH_2BrCl have been calculated using multiconfigurational CASSCF, second-order perturbation theory CASPT2 and its multistate extension MS-CASPT2. The CASSCF method shows spurious valence–Rydberg mixing and a wrong order of states. Inclusion of dynamical correlation by single root CASPT2 lowers dramatically the energy of the valences states but does not lead to a complete separation between valence and Rydberg states. This situation is improved by the MS-CASPT2 calculations, which gives two valence states for both A' and A'' symmetries below the lowest Rydberg state, corresponding to $n(\mathrm{Br}) \rightarrow \sigma^*(\mathrm{C–Br})$ and $n(\mathrm{Cl}) \rightarrow \sigma^*(\mathrm{C–Cl})$ transitions at 6.1 eV (203 nm) and 7.2 eV (173 nm), and being repulsive along C–Br and C–Cl coordinates.

1. Introduction

Chlorobromomethane, CH_2BrCl, is a natural gas released by oceanic losses [1] which together with other biogenic halocarbons contributes to the active bromine in the Earth's atmosphere. The basic oxidation reactions for CH_2BrCl removal are reactions with hydroxil radicals and solar ultraviolet (UV) photolysis, leading to an overall atmospheric lifetime of 0.21 years [2]. Solar photolysis is not particularly significant in the troposphere, but it is a plausible loss mechanism in the stratosphere, where halogen atoms are well known to contribute to ozone depletion [3]. Still, atomic bromine shows a 40 times more powerful ozone depletion potential [4] than the chlorine atom [5] and for that reason bromine containing compounds have attracted an increasing interest in the atmospheric chemistry community [2,6–11]. Additional interest on CH_2BrCl comes from its industrial applications as a possible replacement for CF_3Br and CF_2ClBr in some fire suppressants.

Besides their environmental importance, halomethanes are subject of fundamental investigations of photodissociation reactions in gas and condensed phase. Under UV light halomethanes are excited to various repulsive states leading to a

* Corresponding author. Fax: +49-30-838-52-097.
E-mail address: leti@chemie.fu-berlin.de (L. González).
[1] Permanent address: Department of Spectroscopy, Institute of Isotope- and Surface Chemistry, CRC, HAS, 1121 Budapest, Konkoly-Thege M. út 29-33., Hungary.

0009-2614/01/$ - see front matter
PII: S0009-2614(01)01273-8

direct carbon–halogen (C–X) bond breaking reaction which typically occurs on a time scale shorter than the rotational period of the parent molecule [12]. Nevertheless, detailed investigations of the photochemistry of halocarbons containing bromine are not extensive. Multihalomethanes have in general a more complicated UV absorption spectra and a greater complexity in the dissociation pathways than their well-studied monohalomethanes analogues.

CH_3X is one of the systems whose photodissociation has been extensively studied from experimental [13–16] and theoretical point of view [17,18]. The general features of its dynamics are well understood, and therefore it serves as a reference to understand other more complicated multihalomethanes. For instance, the absorption profile and dynamic properties of CH_3Br have been used to deduce those of CH_2BrCl [9,13,16,19]. Thus, the absorption peak at 203 nm assigned to the $n(\mathrm{Br}) \rightarrow \sigma^*(\mathrm{C–Br})$ transition in CH_3Br has been predicted to occur at the same wavelength in CH_2BrCl [19]. In agreement to this fact, UV absorption cross-sections of CH_2BrCl have been measured recently finding a maximum at 202.6 ± 0.5 nm [2]. Unfortunately, no absorption spectrum below 180 nm is yet reported, therefore the absorption peak due to $n(\mathrm{Cl}) \rightarrow \sigma^*(\mathrm{C–Cl})$ could only be estimated near 164 nm by comparison of that of CF_2BrCl, which shows an absorption peak at this wavelength [20].

Since early investigations, the photolysis of the two bonds C–Br and C–Cl in CH_2BrCl have been suggested to be possible, although the C–Cl breaking only around wavelenghts of ca. 200 nm [21]. Later investigations using translational spectroscopy have shown that at 248 nm CH_2BrCl undergoes exclusively C–Br dissociation, while at 193 nm both C–Br and C–Cl fragmentations are detected with a branching ratio of 4.5 in favour of C–Br against C–Cl fission [6]. A more detailed state-resolved ion time-of-flight mass spectroscopy has been reported in the range 248–268 nm indicating only elimination of the bromine atom, [8] while between 193 and 242 nm one finds a contribution from the $n(\mathrm{Cl}) \rightarrow \sigma^*(\mathrm{C–Cl})$ transition [9]. Furthermore, to verify the character of the ground and excited state halogen atoms and separate the possible influence of the other chromophore, the photodissociation dynamics of CH_2BrCl has been studied at 234 nm using molecular beam-imaging and again C–Br bond cleavage was the only one observed [10].

Despite of all the experimental interest raised by CH_2BrCl, no theoretical studies have been carried out for this molecule or similar dihalomethanes. Here, we report the first high-level ab initio results of transitions to the low-lying singlet states of CH_2BrCl through multiconfigurational CASSCF/MS-CASPT2 calculations as a first step towards elucidating the photodissociation pathways of CH_2BrCl and as a guide for similar chromophores.

2. Computational details

The equilibrium geometry for the ground state of CH_2BrCl has been determined at the MP2(fc)/6-311+G(d,p) level of theory. The relevant geometrical parameters are shown in Fig. 1. Using this optimized geometry the vertical excitation energies for the lowest singlet excited states and their relative transition dipole moments have been calculated using multiconfigurational methods. The calculations have been carried out within the C_s symmetry constraint, with the Br atom placed in the z axis and the Cl in the xz plane (cf. Fig. 1).

Generally contracted basis sets of the Atomic Natural Orbital (ANO-L) type were employed for C, H and Cl atoms [22], whereas a relativistic effective core potential (ECP) approximation was

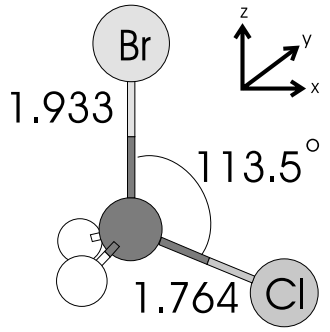

Fig. 1. Equilibrium ground state structure of CH_2BrCl optimized at MP2/6-311+G(d,p) level of theory, together with its molecular orientation. Distances in Angstroms and angles in degrees.

used for the Br atom. Specifically, the following contraction schemes were used: a (14s9p4d) set contracted to [4s3p2d] for the C atom, a (8s4p)/[3s2p] set for the H atoms, a (17s12p5d)/[5s4p2d] set for the Cl atom and the AIMP (9s8p4d)/[3s4p2d] ($Z = 7.0$) ECP [23] for the Br atom. The ANO-L basis sets are designed to treat correlation and polarization effects in an optimal way so they should be large enough to calculate the excitation energies as accurately as possible. To describe correctly not only valence states but also the low-energy Rydberg states the former valence basis sets for C, Cl and Br have been augmented with an extra set of 2s′2p′1d′ diffuse functions constructed from the primitive uncontracted set, with exponents generated following the standard procedure devised by Kaufman et al. [24]. A total number of 132 basis functions are comprised in the calculations.

Initially, the reference wave functions and molecular orbitals have been determined from state-averaged CASSCF (SA-CASSCF) calculations of a given symmetry and spin. To account for dynamical correlation these wave functions were used in subsequent multistate second-order perturbation CASPT2 treatment (MS-CASPT2)[25]. The MS-CASPT2 approach uses a multidimensional reference space by coupling simultaneously different single root SS-CASPT2 states [26] of the same symmetry previously included in the SA-CASSCF wave function. It has been shown that in this way nearly degeneracies can be described correctly and possible erroneous valence–Rydberg mixing can be removed. Examples of strong valence–Rydberg interaction at CASSCF level are the excited states of ethene, butadiene or *n*-tetrasilane [25,27,28]. In all cases the MS-CASPT2 method was able to separate effectively the computed states which could be then clearly identified as either valence or Rydberg states.

In the CASSCF spectrum some valence excited states may be misplaced at considerably high energies. Since the inclusion of dynamical correlation can drastically alter the order of the states when going from CASSCF to SS-CASPT2, it is therefore necessary to include a sufficient number of states in the SA-CASSCF wave function to guarantee that no low-lying state is missing at the CASPT2 level. Based on a large number of testing calculations we have determined that in order to describe the low-energy valence states for the CH_2BrCl and obtain a balanced description of the mixing in the zero-order wave function, 11 roots of A′ symmetry and 10 roots of A″ symmetry are to be included. The active space used in the SA-CASSCF calculation contains 12 electrons correlated in 12 orbitals, including the molecular orbitals from 9a′ to 16a′, and from 3a″ to 6a″, which correspond to the σ, σ^*(C–Br), σ, σ^*(C–Cl), n_z(Cl), n_x(Br), n_y(Cl), n_y(Br), plus Rydberg orbitals. The a^1A' electronic ground state configuration conforms to a closed shell occupation $(9a')^2\ (10a')^2\ (11a')^2\ (12a')^2\ (3a'')^2\ (4a'')^2\ (13a')^0\ (14a')^0$ corresponding to a $\sigma(\text{C–Cl})^2\ \sigma(\text{C–Br})^2\ n_z(\text{C l})^2\ n_x(\text{B r})^2\ n_y(\text{C l})^2\ n_y(\text{B r})^2\ \sigma^*(\text{C–C l})^0\ \sigma^*(\text{C–B r})^0$ configuration.

A well-known problem in CASPT2 is the occurrence of intruder states, which is more critical when a large number of diffuse functions are used in the basis set [29]. The best way to remove intruder states is to increase the active space, such that the intruder states are moved into the CAS CI space. However, in the present case the active space is close to practical limitations, therefore the level shift technique had to be used [30]. After a careful analysis it was found that with a value of $\text{LS} = 0.3$ reliable CASSCF reference weights ω in the CASPT2 calculation are obtained and the correlated energies are converged.

The CASSCF state interaction method [31] was used to calculate the transition dipole moments μ_{ij} from the corresponding perturbed-modified CAS (PMCAS) reference function [25], that is, linear combinations of all CAS states involved in the MS-CASPT2 calculation. The oscillator strength is calculated as $2/3\mu_{ij}^2\Delta E$ using the energy differences ΔE obtained at the MS-CASPT2 level.

All the CASSCF/MS-CASPT2 calculations were carried out using the MOLCAS 5.0 quantum chemistry software [32] while MP2 calculations were performed with the GAUSSIAN 98 package of programs [33].

3. Results and discussion

The structure of CH_2BrCl optimized at the MP2/6-311+G(d,p) level of theory is shown in Fig.

1. There are significant differences between the MP2/6-31G values previously reported in the literature [10] concerning the C–Br and C–Cl distances, and the ones obtained in this work, which are shortened by ca. 0.1 Å. No experimental structure is available, but the experimental vibrational frequencies [34] and those calculated at MP2/6-311+G(d,p) and scaled by the empirical factor 0.9646 [35] (see Table 1) are in a very good agreement (<2% error), validating our molecular structure.

The vertical excitation energies of the singlet valence and Rydberg excited states of A′ symmetry of CH_2BrCl obtained by CASSCF and SS-CASPT2 calculations, together with the composition of the wave function, the expectation value of the total second cartesian moments, R^2 (which serve to differentiate valence from Rydberg states), and the corresponding oscillator strengths, f, are collected in Table 2. The last column contains the weight of the reference wave function (CASSCF) in the first-order perturbed approach. In all cases the values are between 0.89 and 0.85 indicating that calculations performed with LS = 0.3 are balanced and most intruder states have been suppressed.

At the CASSCF level there is a considerable mixing of valence and Rydberg states in the first five excitations. In Table 2, only those configurations with a coefficient higher than 0.4 are reported. Nevertheless a small fraction of a Rydberg transition is also present in the b^1A' state, as well as small contributions of valence states are present in the c^1A' and d^1A' states at CASSCF level, not shown in the table, indicating a deficient description of the low-lying spectrum at this level of theory. The values of R^2 also reflect this valence–Rydberg mixing. The values for the valence states are expected to be close to the ground state value of 73 a.u., whereas values for the second moments in Rydberg states vary from 120 to 200 a.u., depending on the character of the Rydberg state. Those denoted by Rydb A′ correspond mainly to an excitation to the 3s orbital, while the Rydb A″ are excitations to different combinations of 3p orbitals.

Table 1
Scaled harmonic vibrational frequencies at the MP2/6-311+G(d,p) level (in cm^{-1}) compared with the experimental ones and its corresponding assignments

Type of mode	Exper.[a]	This work
Br–C–Cl bending	229	230
C–Br stretching	614	617
C–Cl stretching	744	764
CH_2 rocking	852	847
CH_2 twisting	1128	1144
CH_2 wagging	1231	1263
CH_2 bending	1482	1416
CH_2 s-stretching	3003	3052
CH_2 a-stretching	3066	3129

[a] Taken from Ref. [34].

The inclusion of dynamical correlation by means of SS-CASPT2 alters dramatically the order of the states, dropping considerably in energy the valence states. See for instance, that the valence state $n_x(Br) \rightarrow \sigma^*(C–Cl)$ in k^1A' at CASSCF level, appears at SS-CASPT2 level much lower in energy and heavily mixed with other valence states, as $n_z(Cl) \rightarrow \sigma^*(C–Br)$ in e^1A' and h^1A' roots. However, single root CASPT2 does not remove all the valence–Rydberg mixing, as it can be observed in the states d^1A' and g^1A'. It is therefore to be expected that the energies provided by the SS-CASPT2 are still not reliable. It is also worth noting that the mixing in the wave function also varies substantially in going from CASSCF to SS-CASPT2.

The results for the A′ and A″ transitions at the highest level of theory employed (MS-CASPT2) are presented in Tables 3 and 4, respectively, together with the PMCAS energies. At this level of theory most of the valence–Rydberg mixing is cleared, as it can be noted in the values of the second moments, R^2, which for the valence states are always close to the ground state value. For the Rydberg states the specific expectation values of the $\langle x^2\rangle$, $\langle y^2\rangle$, $\langle z^2\rangle$ are also given, in order to identify the polarization of the Rydberg transitions. The oscillator strengths of the respective states should also encompass the differences between valence and Rydberg states. Typically, Rydberg states possess transition dipole moments smaller than the valence states, since the overlap between atomic orbitals and valence orbitals is less effective than the overlap between two valence orbitals. In this case, however, some Rydberg

Table 2
CASSCF and SS-CASPT2 calculated excitation energies with their corresponding one-electron excitations (weighting coefficients in parenthesis), expectation values of R^2, oscillator strengths f, and weight of the reference CASSCF function ω, for the states of A′ symmetry of CH_2BrCl

Transition	CASSCF					SS-CASPT2			
	Principal conf.		ΔE (eV)	$\langle R^2\rangle$[a]	f	Principal conf.		ΔE (eV)	ω[b]
$a^1A' \rightarrow b^1A'$	$n_x(Br) \rightarrow \sigma^*(C–Br)$ $n_z(Cl) \rightarrow \sigma^*(C–Br)$	(−0.71) (−0.47)	6.92	81.9	0.0036	$n_x(Br) \rightarrow \sigma^*(C–Br)$	(0.83)	6.20	0.874
$a^1A' \rightarrow c^1A'$	$n_x(Br) \rightarrow$ Rydb A′ $n_z(Cl) \rightarrow$ Rydb A′	(0.66) (−0.60)	7.57	115.7	0.0295	$n_x(Br) \rightarrow$ Rydb A′	(0.85)	7.35	0.879
$a^1A' \rightarrow d^1A'$	$n_y(Br) \rightarrow$ Rydb A″(2) $n_y(Cl) \rightarrow$ Rydb A″(1)	(−0.54) (0.51)	8.13	140.9	0.0081	$n_z(Cl) \rightarrow \sigma^*(C–Cl)$ $n_y(Br) \rightarrow$ Rydb A″(1)	(−0.62) (0.38)	7.68	0.873
$a^1A' \rightarrow e^1A'$	$n_x(Br) \rightarrow$ Rydb A″(1) $n_z(Cl) \rightarrow$ Rydb A′ $n_z(Cl) \rightarrow \sigma^*(C–Br)$	(−0.48) (−0.44) (−0.42)	8.29	108.3	0.0118	$n_z(Cl) \rightarrow \sigma^*(C–Br)$ $n_x(Br) \rightarrow \sigma^*(C–Cl)$	(−0.70) (−0.55)	7.74	0.852
$a^1A' \rightarrow f^1A'$	$n_z(Cl) \rightarrow$ Rydb A′ $n_z(Cl) \rightarrow \sigma^*(C–Cl)$ $n_z(Cl) \rightarrow \sigma^*(C–Br)$	(−0.52) (−0.51) (0.42)	8.72	97.0	0.0212	$n_z(Cl) \rightarrow$ Rydb A′	(0.67)	7.86	0.870
$a^1A' \rightarrow g^1A'$	$n_y(Cl) \rightarrow$ Rydb A″(2) $n_y(Cl) \rightarrow$ Rydb A″(1) $n_y(Br) \rightarrow$ Rydb A″(1)	(0.66) (0.49) (−0.45)	8.99	196.6	0.0351	$n_y(Br) \rightarrow$ Rydb A″(1) $n_z(Cl) \rightarrow \sigma^*(C–Cl)$	(0.85) (−0.30)	8.06	0.881
$a^1A' \rightarrow h^1A'$	$n_y(Br) \rightarrow$ Rydb A″(2) $n_y(Cl) \rightarrow$ Rydb A″(1)	(−0.75) (0.40)	9.13	148.0	0.0126	$n_x(Br) \rightarrow \sigma^*(C–Cl)$ $n_z(Cl) \rightarrow \sigma^*(C–Br)$	(0.76) (−0.32)	8.62	0.847
$a^1A' \rightarrow i^1A'$	$n_z(Cl) \rightarrow \sigma^*(C–Cl)$ $n_x(Br) \rightarrow \sigma^*(C–Br)$	(−0.64) (−0.43)	9.57	76.0	0.0176	$n_y(Br) \rightarrow$ Rydb A″(2)	(0.89)	9.09	0.884
$a^1A' \rightarrow j^1A'$	$n_y(Br) \rightarrow$ Rydb A″(1) $n_z(Cl) \rightarrow$ Rydb A″(1) $n_y(Br) \rightarrow$ Rydb A″(2)	(−0.68) (−0.42) (−0.40)	9.85	192.5	0.0113	$n_y(Cl) \rightarrow$ Rydb A″(1)	(−0.92)	9.12	0.880
$a^1A' \rightarrow k^1A'$	$n_x(Br) \rightarrow \sigma^*(C–Cl)$	(0.74)	10.62	81.6	0.1732	$n_y(Cl) \rightarrow$ Rydb A″(2)	(−0.94)	9.80	0.878

[a] For the ground state $\langle R^2\rangle = 72.7$.
[b] For the ground state $\omega = 0.889$.

Table 3
PMCAS and MS-CASPT2 calculated excitation energies (eV) with the corresponding main one-electron excitation, expectation values of R^2 (the specific expectation values of x^2, y^2 and z^2 for the Rydberg states are given in parenthesis), and oscillator strengths f, for the states of A′ symmetry of CH_2BrCl

Transition	Principal conf.	Excitation energy (eV)		$\langle R^2\rangle$[a]	f
		PMCAS	MS-CASPT2		
$a^1A' \rightarrow b^1A'$	$n_x(Br) \rightarrow \sigma^*(C–Br)$	6.98	6.12	76.2	0.0071
$a^1A' \rightarrow c^1A'$	$n_z(Cl) \rightarrow \sigma^*(C–Cl)$	7.66	7.18	74.9	0.0207
$a^1A' \rightarrow d^1A'$	$n_x(Br) \rightarrow$ Rydb A′	8.29	7.42	118.5 (37.4, 44.1, 37.0)	0.0385
$a^1A' \rightarrow e^1A'$	$n_z(Cl) \rightarrow \sigma^*(C–Br)$	8.48	7.79	79.1	0.0023
$a^1A' \rightarrow f^1A'$	$n_z(Cl) \rightarrow$ Rydb A′	8.52	8.15	125.1 (38.7, 50.5, 35.9)	0.0233
$a^1A' \rightarrow g^1A'$	$n_y(Br) \rightarrow$ Rydb A″(1)	9.03	8.19	142.4 (40.3, 64.3, 37.8)	0.0033
$a^1A' \rightarrow h^1A'$	$n_x(Br) \rightarrow \sigma^*(C–Cl)$	9.11	8.59	77.7	0.1567
$a^1A' \rightarrow i^1A'$	$n_y(Br) \rightarrow$ Rydb A″(2)	9.33	9.09	173.8 (57.3, 76.2, 40.3)	0.0349
$a^1A' \rightarrow j^1A'$	$n_y(Cl) \rightarrow$ Rydb A″(1)	9.88	9.16	173.6 (57.3, 75.7, 40.6)	0.0003
$a^1A' \rightarrow k^1A'$	$n_y(Cl) \rightarrow$ Rydb A″(2)	10.47	9.88	197.6 (76.6, 79.4, 41.6)	0.0002

[a] For the ground state $\langle X^2\rangle = 24.3$, $\langle Y^2\rangle = 24.8$, $\langle Z^2\rangle = 23.6$, $\langle R^2\rangle = 72.7$.

states still show very intense bands. Although at the MS-CASPT2 level all the states can be identified with an almost pure excitation, still some mixing of states is present to a minor extent. It could be that still the present level of theory presents some artificial valence–Rydberg mixing or that the valence transitions for this molecule are very weak. Nevertheless, there is an evident correction on the ordering of the states predicted by the MS-CASPT2 energies and on the composition of the PMCAS wave function in comparison with the single root perturbed method. To best appreciate the effect of the dynamical correlation on the CASSCF wave function through single root or multistate CASPT2, the evolution of the main contribution of the wave function of each A′ state along with its corresponding vertical excitation energy at the three different levels of theory calculated in this work: CASSCF, SS-CASPT2 and MS-CASPT2, is illustrated in Fig. 2. As one can see, MS-CASPT2 includes most dynamical correlation, as seen from the energy lowering with respect to the CASSCF values, which in some cases is enough to reverse the order of some states with respect to the order predicted by SS-CASPT2. These differences between single root and multistate CASPT2 may also reflect the artifacts of the approximation implicit in using SS-CASPT2 from SA-CASSCF orbitals. This is specially critical when the starting reference CASSCF wave function is not correct due to second-order energy coupling terms between various electronic states, as it is the case when valence–Rydberg mixing is present at CASSCF level.

According to Tables 3 and 4, in both symmetries two valence excited states occur below the lowest Rydberg state. They correspond to the transitions $n_x(Br) \rightarrow \sigma^*(C–Br)$ calculated at 6.12 eV and $n_z(Cl) \rightarrow \sigma^*(C–Cl)$ lying at 7.18 eV in A′ symmetry and $n_y(Br) \rightarrow \sigma^*(C–Br)$ at 6.04 eV and $n_y(Cl) \rightarrow \sigma^*(C–Cl)$ at 7.11 eV in A″ symmetry. According to Orkin et al. [2] the experimental UV

Table 4
PMCAS and MS-CASPT2 calculated excitation energies (eV) with the corresponding main one-electron excitation, expectation values of R^2 (the specific expectation values of x^2, y^2 and z^2 for the Rydberg states are given in parenthesis), and oscillator strengths f, for the states of A″ symmetry of CH_2BrCl

Transition	Principal conf.	Excitation energy (eV)		$\langle R^2\rangle$[a]	f
		PMCAS	MS-CASPT2		
$a^1A' \rightarrow a^1A''$	$n_y(Br) \rightarrow \sigma^*(C–Br)$	7.02	6.04	81.7	0.0078
$a^1A' \rightarrow b^1A''$	$n_y(Cl) \rightarrow \sigma^*(C–Cl)$	7.60	7.11	78.5	0.0049
$a^1A' \rightarrow c^1A''$	$n_y(Br) \rightarrow$ Rydb A′	8.26	7.40	125.7 (38.1, 49.46, 38.0)	0.0442
$a^1A' \rightarrow d^1A''$	$n_y(Cl) \rightarrow \sigma^*(C–Br)$	8.28	7.86	95.9	0.0014
$a^1A' \rightarrow e^1A''$	$n_x(Br) \rightarrow$ Rydb A″(1)	8.46	8.17	146.2 (38.7, 70.5, 37.0)	0.0010
$a^1A' \rightarrow f^1A''$	$n_y(Cl) \rightarrow$ Rydb A′	9.05	8.22	129.9 (37.4, 56.8, 35.7)	0.0009
$a^1A' \rightarrow g^1A''$	$n_y(Br) \rightarrow \sigma^*(C–Cl)$	9.06	8.48	81.7	0.0024
$a^1A' \rightarrow h^1A''$	$n_z(Cl) \rightarrow$ Rydb A″(1)	9.57	9.05	163.7 (46.5, 80.6, 36.6)	0.0006
$a^1A' \rightarrow i^1A''$	$n_x(Br) \rightarrow$ Rydb A″(2)	9.88	9.16	193.2 (66.3, 84.9, 42.0)	0.0166
$a^1A' \rightarrow j^1A''$	$n_z(Cl) \rightarrow$ Rydb A″(2)	9.97	9.83	203.3 (75.8, 86.5, 41.0)	0.0047

[a] For the ground state $\langle X^2\rangle = 24.3$, $\langle Y^2\rangle = 24.8$, $\langle Z^2\rangle = 23.6$, $\langle R^2\rangle = 72.7$.

spectrum of CH_2BrCl has a maximum cross-section at 202.6 ± 0.5 nm (6.1 eV) which according to the MS-CASPT2 results can be assigned to $n(Br) \rightarrow \sigma^*(C–Br)$ transitions. These states were placed by SS-CASPT2 higher by ca. 0.1 eV. No absorption cross-sections were measured below 187 nm, but the experimental absorption profile shows an increasing tendency starting at 192 nm, which according to our results must correspond to the onset of the $n_z(Cl) \rightarrow \sigma^*(C–Cl)$ absorption band. According to this assignment, the $n(Cl) \rightarrow \sigma^*(C–Cl)$ band appears at higher wavelengths (173 nm) than it can be estimated from CF_2BrCl (164 nm) [20]. At 7.4 eV lies the lowest Rydberg state $n(Br) \rightarrow$ Rydb A′, almost degenerated in both symmetries, with a predicted oscillator strength of 0.04. The nature of the transitions in the A′ and A″ spectrum are very similar in the light of the two near-degenerate lone pair molecular orbitals, and since the A′ counterparts show more intense peaks than the A″ ones, from now on we will focus mostly on the A′ transitions. Another shoulder should be present in the spectrum at 7.8 eV due to the e^1A' state designated as $n_z(Cl) \rightarrow \sigma^*(C–Br)$ transition. In the present assignment the PMCAS oscillator strength is very weak, cf. Table 3. One reason for that could be that this state comes from the SS-CASPT2 e^1A' state computed with a reference weight of 0.85, low in comparison with the ground state value 0.89. The next electronic transitions are two Rydberg states from the Cl and Br lone pairs, in increasing order of energy, respectively. They conform the f^1A' and g^1A' or e^1A'' and f^1A'' states, predicted almost degenerated at ca. 8.2 eV, in both A′ and A″ symmetries. These states are placed by MS-CASPT2 ca. 0.3 eV higher in energy with respect to the single root CASPT2, to compensate the decrease of energy in the valence states lying below (cf. Fig. 2). The next valence state, h^1A', corresponding to the $n_x(Br) \rightarrow \sigma^*(C–Cl)$ transition, is predicted very

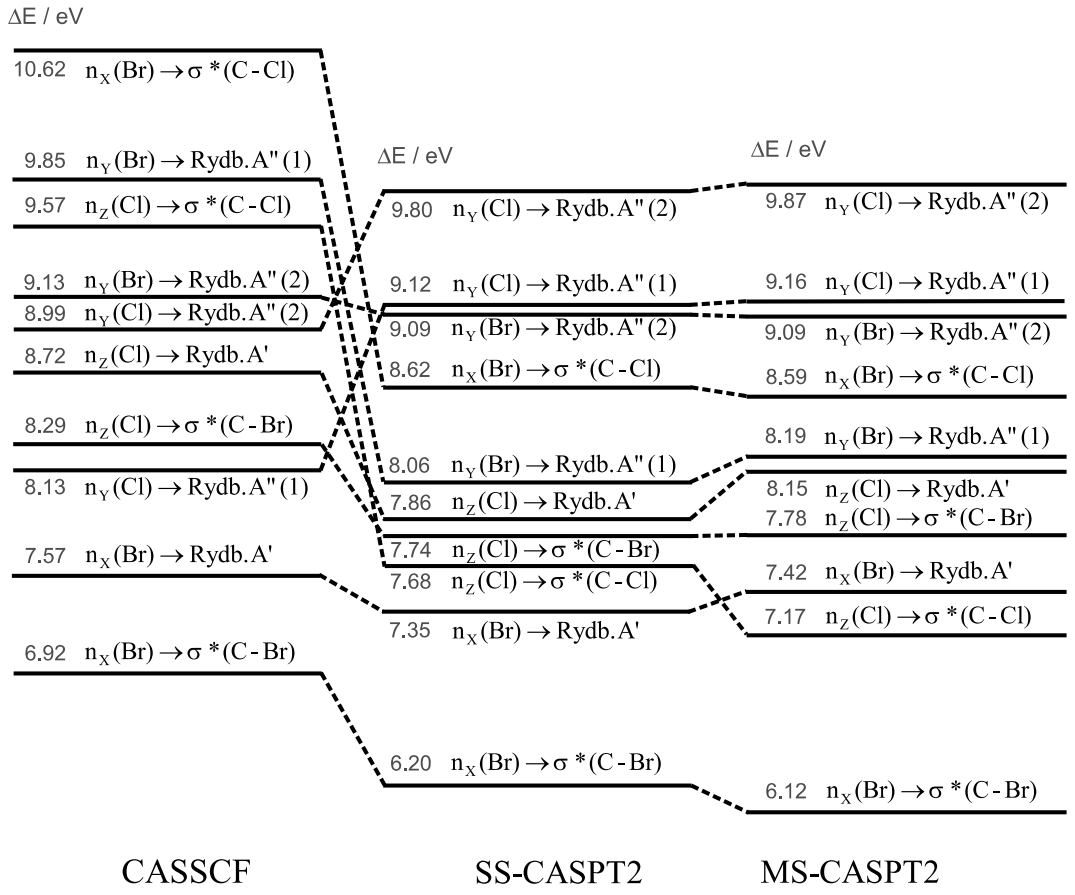

Fig. 2. Schematic representation of the change in energy of the excited states and corresponding wave function of the A′ states when going from CASSCF, to SS-CASPT2 and MS-CASPT2 level of theory. (Only the excitation with the main contribution on the wave function is shown for each root.)

intense at both MS-CASPT2 (see Table 3) and CASSCF level (see k^1A' in Table 2), with an oscillator strength of ca. 0.15. This state is calculated at 8.6 eV, at both single and multistate CASPT2 level. At higher energies, above 9 eV, lie three different Rydberg states with decreasing oscillator strengths, suggesting that these states should have little or no contribution to the absorption spectrum.

All the calculated valence transitions in CH_2BrCl involve promotions from the lone pairs of the Cl or Br atoms to the antibonding σ^* orbitals on the C–X bond. These excitations are generally repulsive, mostly leading to direct C–X bond cleavage. MS-CASPT2 calculations along the C–Cl and C–Br coordinates to confirm the nature of the potetial energy curves are in progress in our group. The lowest states, corresponding to $n(Br) \rightarrow \sigma^*(C–Br)$ and $n(Cl) \rightarrow \sigma^*(C–Cl)$ transitions along the C–Br and C–Cl coordinates, respectively, are strongly repulsive and cross at certain point, which implies that absorption into these states should lead to direct and fast photodissociation producing corresponding CH_2Cl and CH_2Br fragments.

4. Conclusion

CASSCF and CASPT2 methods have been applied to calculate the vertical excitations ener-

gies of the low-lying electronic excited states of the CH_2BrCl molecule for the first time. The CASSCF wave function contains a strong valence–Rydberg mixing which is not completely removed with single root CASPT2 calculations, indicating that the energetics at those levels of theory are not reliable. Nevertheless, the inclusion of dynamical correlation had a very strong effect on the energetics, revesing the order of the states dramatically with respect to the zero-order wave function, specially the valence states with respect to the Rydberg ones. This was particularly true for multistate-CASPT2, which has demonstrated to be capable of correcting errors obtained at SS-CASPT2 level.

Two valence states for both A' and A'' symmetries are then found at the MS-CASPT2 level below the lowest Rydberg transition. Each can be assigned to a main excitation from a lone pair of the halogen atom to the valence antibonding σ^* of the C–X bond. The first state corresponds to $n(\mathrm{Br}) \rightarrow \sigma^*(\mathrm{C–Br})$, calculated at 6.1 eV (203 nm), which is in very good agreement with the experimental peak of the UV spectrum found at 202.6 nm by Orkin et al. [2]. The second one is attributed to a $n(\mathrm{Cl}) \rightarrow \sigma^*(\mathrm{C–Cl})$ and placed at 7.2 eV (173 nm). The lowest excited state along the respective C–Br and C–Cl coordinates is strongly repulsive, leading to the fast formation of CH_2Cl and CH_2Br fragments and atomic Br and Cl, respectively.

Acknowledgements

We would like to express our deep thanks to Prof. M. Merchán for her patient explanations about Rydberg states and MS-CASPT2 calculations. Generous financial support by the Deutsche Forschungsgemeinschaft DFG is gratefully acknowledged (T.R., T.F.). All calculations have been performed on HP workstations of the Theoretische Chemie group, Freie Universität Berlin.

References

[1] D.J. Wubbles, A.K. Jain, K.O. Patten, P.S. Connell, Atmos. Environ. 32 (1997) 107.
[2] V.L. Orkin, V.G. Khamagonov, A.G. Guschin, R.E. Huie, M.J. Kurylo, J. Phys. Chem. 101 (1997) 174.
[3] R. Vogt, P.J. Crutzen, R. Sander, Nature 383 (1996) 327.
[4] R.P. Wayne, in: The Chemistry of Atmospheres, second ed., Oxford University, New York, 1991, and references therein.
[5] S.C. Wofsy, M.B. McElroy, Y.L. Yong, Geophys. Res. Lett. 2 (1975) 215.
[6] W.B. Tzeng, Y.R. Lee, S.M. Lin, Chem. Phys. Lett. 227 (1994) 467.
[7] M. Bilde, J.W.T.C. Ferronato, J.J. Orlando, G.S. Tyndall, E. Estupinan, S. Haberkorn, J. Phys. Chem. A 102 (1998) 1976.
[8] W.S. McGivern, R. Li, P. Zou, S.W. North, J. Chem. Phys. 111 (1999) 5771.
[9] P. Zou, W.S. McGivern, S.W. North, Phys. Chem. Chem. Phys. 2 (2000) 3785.
[10] S.-H. Lee, Y.-J. Jung, K.-H. Jung, Chem. Phys. 260 (2000) 143.
[11] Y. Lin, J.S. Francisco, J. Chem. Phys. 114 (2001) 2879.
[12] L.J. Butler, E.J. Hintsa, Y.T. Lee, J. Chem. Phys. 86 (1987) 2051.
[13] G.N.A. van Veen, T. Baller, A.E. de Vries, Chem. Phys. 92 (1985) 59.
[14] W.P. Hess, D.W. Chandler, J.W. Thoman Jr., Chem. Phys. 163 (1992) 277.
[15] D.H. Fairbrother, K.A. Briggmann, E. Weitz, P.C. Stair, J. Chem. Phys. 101 (1994) 3787.
[16] T. Gougousi, P.C. Samartzis, T.N. Kitsopoulos, J. Chem. Phys. 108 (1998) 5742.
[17] H. Guo, G.C. Schatz, J. Chem. Phys. 93 (1990) 393.
[18] Y. Amatatsu, S. Yabushita, K. Morokuma, J. Chem. Phys. 104 (1996) 9783, and references therein.
[19] P. Cadman, J.P. Simons, Trans. Faraday Soc. 62 (1966) 631.
[20] J. Doucet, R. Gilbert, P. Sauvageau, C. Sandorfy, J. Chem. Phys. 62 (1975) 366.
[21] R.C. Mitchell, J.P. Simons, Discuss. Faraday Soc. 44 (1967) 208.
[22] P.-O. Widmark, P.-A. Malmqvist, B.O. Roos, Theoret. Chim. Acta 77 (1990) 291.
[23] Z. Barandiarán, L. Seijo, Can. J. Chem. 70 (1992) 409.
[24] K. Kaufmann, W. Baumeister, M. Jungen, J. Phys. B: At. Mol. Opt. Phys. 22 (1989) 2223.
[25] J. Finley, P.-A. Malmqvist, B.O. Roos, L. Serrano-Andrés, Chem. Phys. Lett. 288 (1998) 299.
[26] K. Andersson, P.-A. Malmqvist, B.O. Roos, J. Chem. Phys. 96 (1992) 1218.
[27] L. Serrano-Andrés, M. Merchán, I. Nebot-Gil, R. Lindh, B.O. Roos, J. Chem. Phys. 98 (1993) 3151.
[28] R. Crespo, M. Merchán, J. Michl, J. Phys. Chem. 104 (2000) 8593.
[29] B.O. Roos, M.P. Fülscher, P.-A. Malmqvist, M. Merchán, L. Serrano-Andrés, in: S.R. Langhoff (Ed.), Quantum Mechanical Electronic Structure Calculations with Chem-

ical Accuracy, vol. 13, Kluwer Academic Publishers, Dordrecht, The Netherlands, 1995, p. 357.
[30] B.O. Roos, K. Andersson, Chem. Phys. Lett. 245 (1995) 215.
[31] P.-A. Malmqvist, B.O. Roos, Chem. Phys. Lett. 155 (1989) 189.
[32] K. Andersson et al., MOLCAS 5.0, University of Lund, Sweden, 2000.
[33] M.J. Frisch et al., GAUSSIAN 98, Revision A, vol. 9, Gaussian Inc., Pittsburgh, PA, 1998.
[34] T. Shimanouchi, in: Tables of Molecular Vibrational Frequencies Consolidated, vol. 1, National Bureau of Standards, 1972.
[35] J.A. Pople, A.P. Scott, M.W. Wong, L. Radom, Isr. J. Chem. 33 (1993) 345.